Planar laser-induced fluorescence imaging of flame heat release rate

— **Source link** ⧉

Phillip H. Paul, Habib N. Najm

Institutions: Sandia National Laboratories

Published on: 01 Jan 1998

Topics: Premixed flame, Laminar flame speed and Planar laser-induced fluorescence

Related papers:

- On the Adequacy of Certain Experimental Observables as Measurements of Flame Burning Rate

- Spatially resolved heat release rate measurements in turbulent premixed flames

- Simultaneous single-shot laser-based imaging of formaldehyde, OH, and temperature in turbulent flames

- Experimental and numerical determination of heat release in counterflow premixed laminar flames

- A Study of Flame Observables in Premixed Methane - Air Flames

SAND--98-8474C

Planar Laser-Induced Fluorescence Imaging of Flame Heat Release Rate

CONF-980804 --

Phillip H. Paul and **Habib N. Najm**
Combustion Research Facility
Sandia National Laboratories
Livermore CA 94550 USA

RECEIVED

MAR 27 1998

OSTI

corresponding author   Phillip H. Paul
phone   (510) 294-1465
fax   (510) 294-2595
email   phpaul@ca.sandia.gov

DISCLAIMER

Planar Laser-Induced Fluorescence Imaging of Flame Heat Release Rate

Phillip H. Paul and **Habib N. Najm**
Combustion Research Facility
Sandia National Laboratories
Livermore CA 94550 USA

Abstract   Local heat release rate represents one of the most interesting experimental observables in the study of unsteady reacting flows. The direct measure of burning or heat release rate as a field variable is not possible. Numerous experimental investigations have relied on inferring this type of information as well as flame front topology from indirect measures which are presumed to be correlated. A recent study has brought into question many of the commonly used flame front marker and burning rate diagnostics. This same study found that the concentration of formyl radical offers the best possibility for measuring flame burning rate. However, primarily due to low concentrations, the fluorescence signal level from formyl is too weak to employ this diagnostic for single-pulse measurements of turbulent reacting flows.

In this paper we describe and demonstrate a new fluorescence-based reaction front imaging diagnostic suitable for single-shot applications. The measurement is based on taking the pixel-by-pixel product of OH and CH_2O planar laser-induced fluorescence images to yield an image closely related to a reaction rate. The spectroscopic and collisional processes affecting the measured signals are discussed and the foundation of the diagnostic, as based on laminar and unsteady flame calculations, is presented. We report the results of applying this diagnostic to the study of a laminar premixed flame subject to an interaction with an isolated line-vortex pair.

Introduction   There is a long history of imaging diagnostics being applied to identify flame-front topology and, more recently, to image heat release rate. These quantities cannot be imaged directly, rather they must be inferred from images of some other physical (e.g. dilatation) or chemical (e.g. chemiluminescence) measure. Recently, Najm *et al.* [1] employed both experimental and computational results to investigate the validity of a number of these techniques. They considered an unsteady curved flame front, specifically, a laminar premixed methane-air flame subjected to an interaction with an isolated line-vortex pair. Their observations may be summarized as follows: chemiluminescence-based methods (e.g. CH*, C_2*, OH* and CO_2* imaging) are not generally reliable measures of turbulent flame front topology much less burning or heat release rate; methods based on imaging OH do not provide sufficient contrast to uniquely identify the flame front and OH concentration is an insensitive indicator of local heat release rate; on the other hand CH concentration is not universally correlated with heat release and CH images may wrongly indicate breaks in the flame surface; finally, unsteady strain and curvature can modify any possible correlation between dilatation and heat release rate. An additional method often used to identify flame front topology involves imaging the disappearance of some added tracer (e.g. PLIF of acetone or Mie scattering of a particulate) which decomposes at elevated temperatures. These methods do provide strong signals but must presuppose a direct spatial relationship between the flame front and the disappearance of the tracer which actually occurs in the preheat zone. PLIF images of acetone as seeded into the fuel (in a non-premixed jet flame) display a much more convoluted 'flame' surface than simultaneously acquired OH images [2]. This is expected since the acetone has a higher Schmidt number and it decomposes in a cooler region subjected to turbulence largely unaffected by the flame.

Najm *et al.* [1] find a temporal and spatial correlation between the concentration of formyl radical (HCO) and heat release rate. They suggest that this occurs because: 1) reaction of HCO (to form H and CO) occurs rapidly compared to its formation rate, thus HCO concentration appears as directly proportional to HCO production rate; 2) for slightly rich to lean flames a substantial fraction of the carbon flows through HCO making HCO a good monitor point for the flow of carbon from fuel to products; and, 3) HCO production is directly dependent on the

3

concentration of CH_2O which in turn is directly dependent on the reaction $CH_3 + O \Leftrightarrow CH_2O + H$ which shows the largest fractional influence on changes in heat release rate. Najm *et al.* [1] demonstrated the ability to image HCO using PLIF in a flow similar to that used here and to that used by Nguyen and Paul [3]. However they were forced to average 100 frames of data to achieve peak signal-to-noise ratios of order 2:1 in the final HCO image. They conclude and we confirm that there is insufficient signal available to apply HCO PLIF as a single-pulse imaging diagnostic as would be required for studies of unsteady reacting flows.

In what follows we investigate possible means to develop an image of reaction rate and to what extent the measurement, or some other related expression, correlates with heat release rate. This is followed by a consideration of LIF in OH and CH_2O. Finally we report the results of applying these diagnostics to the study of an unsteady premixed flame.

Heat Release Rate   Our investigations into the causes for the success of HCO as a measure of heat release rate prompted us to consider other means to image reaction rates associated with HCO production. Images of the concentration of a species that is formed at a finite rate but removed rapidly by reaction (e.g. HCO) or by physical quenching of electronically excited species (e.g. $^1CH_2$) offer a measure of the production rate of the species. However this desirable feature also leads to a relatively low concentration of the target species hence unusable signal levels. An alternative is to derive a processed image that is a direct measure of a reaction rate. The reaction $CH_2O + OH \Rightarrow H_2O + HCO$ proceeds at a forward rate proportional to $R_{OH} \propto n_{CH2O} n_{OH} k_f(T)$ where n is a number density and k_f is a rate coefficient. We will show that the product of OH and CH_2O LIF signals taken at the same spatial location may be written as $S_{OH} S_{CH2O} \propto n_{CH2O} n_{OH} g(T)$ where $g(T)$ is a known function of temperature. The actual temperature dependence in $g(T)$ can be adjusted through the selection of the particular transitions being used for the measurement. Over a limited temperature range it is possible to select the transitions such that $g(T)$ sufficiently mimics $k_f(T)$ that the product of the signals is directly proportional to the reaction rate.

Figure 1 shows a comparison of peak heat release rate, HCO concentration and the product of OH and CH_2O concentrations taken on the centerline of a 2D counter-rotating vortex-pair colliding with a laminar premixed methane-air flame [4]. The computed results show an

4

excellent spatial and temporal correlation between heat release rate and the measure $M \propto n_{CH2O}n_{OH}$ which is directly related to the rate R_{OH}. The correlation between heat release rate and the rate R_{OH} can be explained using the same lines of reasoning offered, by Najm *et al.* [1] and outlined above, to explain the correlation between heat release rate and HCO concentration.

Figure 2 shows a comparison of peak-normalized profiles taken from the results of a freely propagating premixed flame calculation ($\phi = 1.0$ methane-air, using GRImech 1.2 [5]), including; dilatation, CH_2O and HCO number densities and the rate R_{OH}. In this figure the rate coefficient used to compute R_{OH} was taken as $k_f = 5.7 \times 10^{-17} \, T^{1.18} \exp(225/T)$ [6]. The dilatation profile delimits the preheat region of the flame which is where the CH_2O is produced, hence the similarity between the two profiles. Also shown in this figure are the product of OH and CH_2O number densities and this product divided by temperature. Over the space where the product $n_{OH}n_{CH2O}$ exists, the temperature variation is sufficiently small that representing $g(T)$ functionally by a constant or by $k_f(T)$ are essentially equivalent whereas the function T^{-1} introduces a slight bias towards the reactants.

LIF of OH and formaldehyde   Under collision dominated conditions (e.g. an atmospheric pressure flame) and in the limit of weak pumping, the laser-induced fluorescence signal takes the form, $S_f \propto X_{abs}f_B(T)A / k_Q(T)$. Here X_{abs} is the mole fraction of the absorbing species having a Boltzmann fraction of $f_B(T)$ in the lower laser-coupled level. The quantities A and $k_Q(T)$ are the spontaneous emission rate and the rate coefficient for collisional de-excitation (physical quenching) of the upper laser-coupled level, respectively. Through a judicious choice of excitation and detection wavelengths it is possible to cancel out much of the temperature dependence and obtain PLIF images of CH or OH that essentially represent mole fraction [3]. Such a simple relation is not the general case, rather the LIF signal is proportional to absorber mole fraction but also contains a complicated dependence on other field variables. For example collisional quenching may exhibit a strong dependence on the identity of the collision partner or on temperature (e.g. NO $A^2\Sigma^+$ [7]), or with polyatomics like formaldehyde there is generally a strong temperature dependence through the Boltzmann fraction.

LIF measurements of native CH_2O in flames have been reported by Harrington and Smyth [8] and PLIF imaging of CH_2O in an engine has been reported by Bauerle et al. [9]. In both cases excitation was via the A^1A_2-X^1A_1 4^1_0 band (near 353 nm). The lifetime of the singlet A-state vibrational levels decreases with increasing energy due to predissociation [10] via a coupling to the lowest triplet surface, a^3A_2 [11], and at higher energies by direct predissociation to H + HCO. Harrington and Smyth [8] suggest that owing to this predissociation, the lowest accessible vibrational level in the A-state will give the strongest fluorescence signal. We find a signal advantage of over 10 times in moving to excitation via the $2^1_04^1_0$ band (near 339 nm). This is due in part to an increase in the absorption coefficient which must be balanced against a predissociation lifetime of 28 ns for the 2^14^1 excited state compared to 85 ns for the 4^1 excited state. However the impact of the increase in predissociation rate is reduced by competitive physical quenching rates [12]. Further the vibration relaxation within the excited state is essentially gas kinetic [12], mitigating against the potential signal loss by transferring population to lower energy, less predissociated vibrational levels. There are also two practical advantages in moving to excitation at 339 nm, the non-resonant emission is more separated from the pump wavelength and is better matched to available colored glass filters, and there is a better match to high performance laser dyes.

A reasonable model for OH LIF signal, using A-X (1,0) excitation and nonresonant fluorescence detection, can be developed owing to the availability of collisional quenching and vibrational relaxation cross sections for a number of collision partners over a wide range of temperatures [13]. The same cannot be said for the first excited singlet of CH_2O for which there is limited collision cross section data, and then only at relatively low temperatures. However the picture of energy transfer in the lower vibrational levels of CH_2O A^1A_2 is one of rapid rotational and vibrational relaxation (nominally 10 times [14] and 2 to 3 times [12] gas kinetic, respectively) as compared to physical quenching and predissociation rates which are of order one-tenth gas kinetic. To develop a model for the CH_2O signal, we assume negligible stimulated emission which is justified because of low intrinsic strength of the A-X transitions (e.g. the $2^1_04^1_0$ band strength is of order 7×10^{-6}) and fast ground [15] and excited state [14] rotational energy transfer (RET) rates. This assumption is confirmed by our measurements and by Harrington and Smyth who observed a linear dependence on laser energy up to fluences of order 3.8 GW/cm^2. Further,

we ignore ground-state bleaching effects because of the rapid RET and the small Boltzmann fraction in the lower laser coupled level, making the lower state rotational bath appear as infinite.

Given the rapid internal collisional energy transfer rates within the excited singlet and the limited collisional energy transfer data base, the simplest model is to assume the excited electronic states are internally in Boltzmann equilibrium. In which case the LIF signal can be written as

$$S_{CH2O} \propto X_{CH2O} \frac{f_B(T)}{k_Q} \sum_i \frac{A_i f_i'(T)}{1 + P_i/k_Q n_o} \qquad (1)$$

where the summation is over all excited vibrational states having Boltzmann fractions and total spontaneous emission rates of $f_i'(T)$ and A_i, respectively. The values of the A_i must be thought of as effective, that is weighted by the spectral response of the detector and filters. Here n_o is the total number density and the P_i are predissociation rates. We have simulated the CH_2O LIF signal using band strengths derived from the tabulations of van Dijk et al. [16], vibrational energies from the review of Clouthier and Ramsey [17], and predissociation and room temperature quenching rates from Moortgat and Warneck [18]. Two models for the temperature dependence in the quenching cross section were considered, temperature independent and power law of the form $T^{-1/2}$. The primary result of these simulations is that any temperature dependence arising from the summation in equation 1 is minor and well within the uncertainty introduced by the assumptions made and the model for the temperature dependence in the quenching cross sections. Simulations were performed for a number of detector spectral response profiles with the best results (weakest temperature dependence) found for detection through 2 to 3 mm of Schott WG-360 or Hoya L-39 filter glass. The simulations suggest that the CH_2O signal can be represented by $S_{CH2O} \propto X_{CH2O} T^{-\beta}$ with $2.2 < \beta < 3$ over the temperature range of 800 to 1800 K using excitation of overlapping transitions in the $^R R_5$ bandhead of the $2^1_0 4^1_0$ system near 338.1 nm. Since $S_{OH} \propto X_{OH}$ the product of the LIF signals can then be written as $S_{OH} S_{CH2O} \propto n_{OH} n_{CH2O} T^{2-\beta}$ thus a functional dependence for $g(T)$ between $T^{-0.2}$ and T^{-1}. The exact functional dependence of $g(T)$ on temperature will depend on the particular transition(s) employed as well as the filter spectral transmission. Given the relatively narrow range of temperatures expected in the region of overlap between OH and CH_2O, the primary field

7

dependence in the product of the LIF signals is through the product of the number densities (see figure 2). Thus the product of the LIF signals provides a measure of a quantity which is correlated with local heat release rate.

Reaction Rate Imaging Results The OH and CH_2O PLIF imaging diagnostics were applied to the study of an unsteady laminar premixed flame. The flow facility is the same as that described by Nguyen and Paul [3]. The burner (63.5 mm square) is packed with glass beads followed by honeycomb and wire screen flow straighteners. The V-flame is stabilized on a slightly heated nichrome wire suspended above the burner. A laminar vortex pair is generated by impulsively driving the premixture through a slot nozzle mounted on one side of the test section. The vortices are injected, at a near-normal angle, into one leg of the V-flame. For this study a slightly lean (ϕ = 0.9) mixture of dimethyl ether was selected to increase CH_2O levels and thus enhance the CH_2O signal. The mixture was diluted with 30% additional N_2 to reduce the flame speed in order to operate under laminar flame and vortex conditions. For the methane - air system, the primary source of CH_2O is oxidation of methyl radical and to a lesser extent by H-abstraction from the methanol-like radicals, CH_3O and CH_2OH. For the dimethyl ether - air system, CH_2O is produced from the thermal decomposition products CH_3O and CH_3 or by H-abstraction to form the methoxy-methyl radical and subsequent β-scission of to yield CH_2O and CH_3 [19]. From the standpoint of CH_2O production this appears like burning a mixture of methanol and methane.

Burner conditions were selected to achieve a highly reproducible flow which allowed the time evolution of the flame-vortex interaction to be mapped out by varying the time delay between firing the vortex generator and firing the lasers and intensifier gates. A flame speed of 10 cm/sec was inferred from the observed V-flame angle and the flow rate of the reactants. The vortex parameters were selected to be the same as those used by Nguyen and Paul [3], specifically, a self-induced velocity of 110 cm/sec and an overall diameter of 0.8 cm. In the present experiment the OH and CH_2O images were not taken simultaneously. Rather, the images were taken sequentially with a single camera to avoid the geometric and signal normalization corrections required for quantitative imaging using two cameras. Two separate laser systems were set up to allow rapid switching between pumping OH and pumping CH_2O.

8

The OH images were obtained using A-X (1,0) Q_1(4.5) excitation (using an XeCl excimer-pumped dye laser doubled in BBO) and non-resonant detection through 2 mm of Schott WG-305 filter glass. The CH_2O images were obtained using excitation at the $^RR_5$ bandhead near 338.1 nm and non-resonant detection through 2.5 mm of Schott WG-360 filter glass. The direct output of an XeCl excimer-pumped dye laser running BiBiQ dye dissolved in propylene carbonate was used, providing nominally 40 mJ per pulse near 338 nm. The images were recorded on a single microchannel plate intensified CCD camera equipped with a 1.5:1 fiber taper and using a pair of El-Nikor enlarging lenses (f/1.8) for the CH_2O and an UV-doublet lens (f/2.4) for the OH. To improve the signal-to-noise, the image data was 3x3 median filtered in post processing.

Figure 3 shows two sets of images taken at 2 and 6 milliseconds into the interaction of the vortex with the flame. In the later OH image there is an indication of the sudden increase or 'burst' in OH signal observed by Nguyen and Paul [3] for conditions of a slightly rich methane - air flame as subject to a similar line vortex pair. They found that this increase in OH was coincident in time with the disappearance of CH around the vortex pair. Under the assumption that CH provides an unambiguous marker of the flame front, Nguyen and Paul were drawn to the conclusion that the action of the vortex pair was to seriously disturb the normal flame chemistry. The present results show the CH_2O surface in contact with the OH surface throughout the interaction. The images in figure 3 show that there is no marked change in peak CH_2O signal along the flame surface indicating that CH_2O concentration is weakly effected by the action of the vortex pair. Further the product images show a continuos reaction front with some decrease in signal, hence in reaction rate. The HCO image results reported by Najm *et al.* for an N_2-diluted methane air flame ($\phi = 1.0$) taken under similar flow and vortex conditions also show an intact reaction surface at a point in the interaction where the CH signal around the vortex pair was observed to be 5 to 10 times less than the undisturbed value (taken nominally one ms earlier into the interaction than the later image set in figure 3).

The OH and CH_2O images given in figure 3 were acquired using single laser pulses. The OH images show a reasonably good signal-to-noise ratio. However the OH signal becomes weak on the reactant side of the flame front in the region of spatial overlap with the CH_2O signal. The CH_2O signal is by comparison weaker, showing a single shot peak signal-to-noise of about 4:1.

Excellent CH$_2$O signal contrast (the ratio of peak signal to that well away from the flame front) was achieved, indicating good rejection of resonant scattering and negligible interference from Raman scattering. However, camera gate widths had to be set to 25 ns to reject flame chemiluminescence. The CH$_2$O rotational constants are relatively large and there is a significant geometry change with excitation, thus the rotational spectrum is relatively open and it is possible to tune off of the excitation line to observe any background signal. Background signal levels in the flame were measured at less than 2% of the observed peak CH$_2$O signal indicating negligible broadband fluorescence interference (e.g. from PAH's).

The convective transport of formaldehyde number density is balanced by mass diffusion and chemical production and removal, at rates P and R, respectively. For the case of minimal tangential gradients, the spatial integral along the flame normal $\hat{r}$ and across the flame surface can be written as

$$\frac{d}{dt}\int_b^u n_{CH2O}dr + \left(n_{CH2O}\hat{r}\bullet\bar{v}\right)\Big|_b^u \cong \int_b^u (P-R)dr \qquad (2)$$

Here the labels u and b refer to unburnt and burnt regions, respectively. For a reaction intermediate like CH$_2$O, the diffusion term vanishes upon integration as will the convective term (in equation 2) for sufficiently large limits of integration. For CH$_2$O, the removal rate is dominated by reactions with H, O and OH to form HCO which implies that $R \geq R_{OH}$. Since HCO concentrations are small the reverse rate (reformation of CH$_2$O from HCO) will also be small. A time series of images can be used to infer a lower bound on the CH$_2$O production rate of the form

$$\int_b^u Pdr \geq \frac{d}{dt}\int_b^u n_{CH2O}dr + \int_b^u R_{OH}dr \qquad (3)$$

This can provide additional information about the state of the reaction system.

Figure 4 shows a set of CH$_2$O LIF signal profiles taken as cuts along the vortex-pair centerline (5 - pixel wide cuts were taken from the image data and averaged laterally). The inset graph shows the time evolution of the spatial integral of the profiles. This indicates a slow monatomic decay in the CH$_2$O signal (inverse exponential in character with a time constant of 5.6 ms), to 82% of the undisturbed value over the 6 ms of flow observed. Figure 5 shows a corresponding graph of

10

the product of the OH and CH$_2$O LIF signals. The integrated profile value drops to 60% of the undisturbed value between 2 and 4 ms. This trend turns around and the integral rises to 75% by 6 ms. This increase is the direct result of the 'burst' in OH LIF signal around the vortex pair which occurs between 5 and 6 ms (see inset in figure 4). As noted above, the CH$_2$O LIF signal and the LIF product image are proportional to the respective integrands on the right-hand side of equation 3 but also retain some additional temperature dependencies. However the first-order interpretation is that the lower bound on CH$_2$O production rate is decreasing with time, the first term (on the right-hand-side of equation 3) is weakly negative and the second term is positive and decreasing in time.

Conclusions   A method for imaging heat release rate and flame front topology has been described and demonstrated. The technique is based on using the product of PLIF images of OH and CH$_2$O to derive an image closely related to a reaction rate. Laminar flame calculations and a simulation of a flame vortex interaction were used to show a correlation between this type of processed image and heat release rate in an unsteady premixed flame vortex interaction. The collisional behavior of the first singlet state of CH$_2$O was reviewed and a relationship for the dependence of CH$_2$O LIF signal on flame field variables was derived.

This new technique was applied to study the transient interaction of an isolated line vortex pair with a premixed laminar dimethyl ether - air flame. The results indicate that that the flame surface is weakly affected by the action of the vortex, both as a C$_{(1)}$ chemistry and as a heat release object. The method has two notable advantages over PLIF imaging of HCO: first the obvious capability to perform single pulse imaging of the reaction front and heat release rate; and second in providing an image of OH along with a joint measure of CH$_2$O concentration and removal rate. The combination of these measurements provides additional insight into the production rates of CH$_2$O and HCO.

The OH - CH$_2$O product imaging technique offers the possibility of reliably imaging the flame front on a single shot basis and thus is suitable for application to turbulent reacting flows. Efforts are underway to refine the model used to describe the CH$_2$O LIF signal, to further refine and test the method, and to optimize the signal-to-noise performance. Application of the technique to study a wider range of unsteady and turbulent reacting flows is in progress.
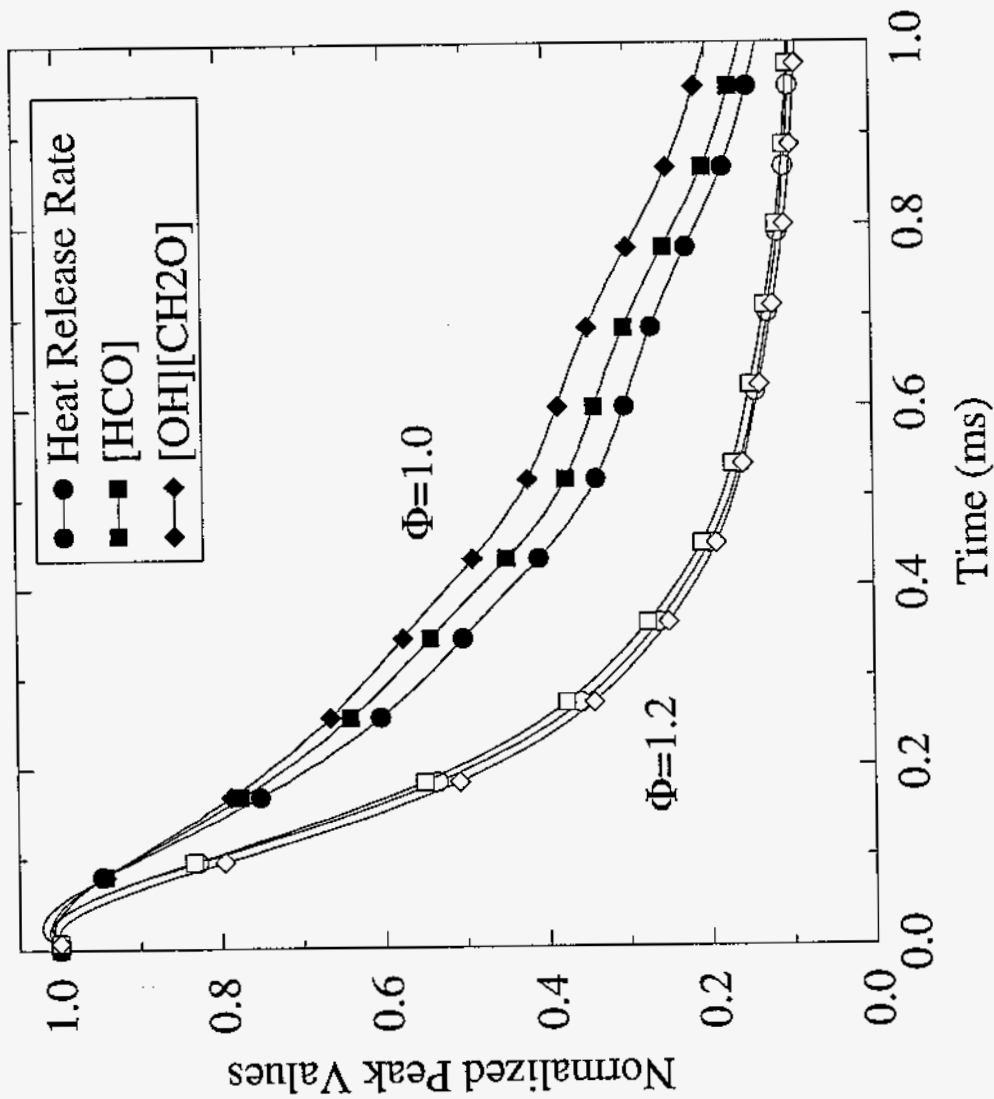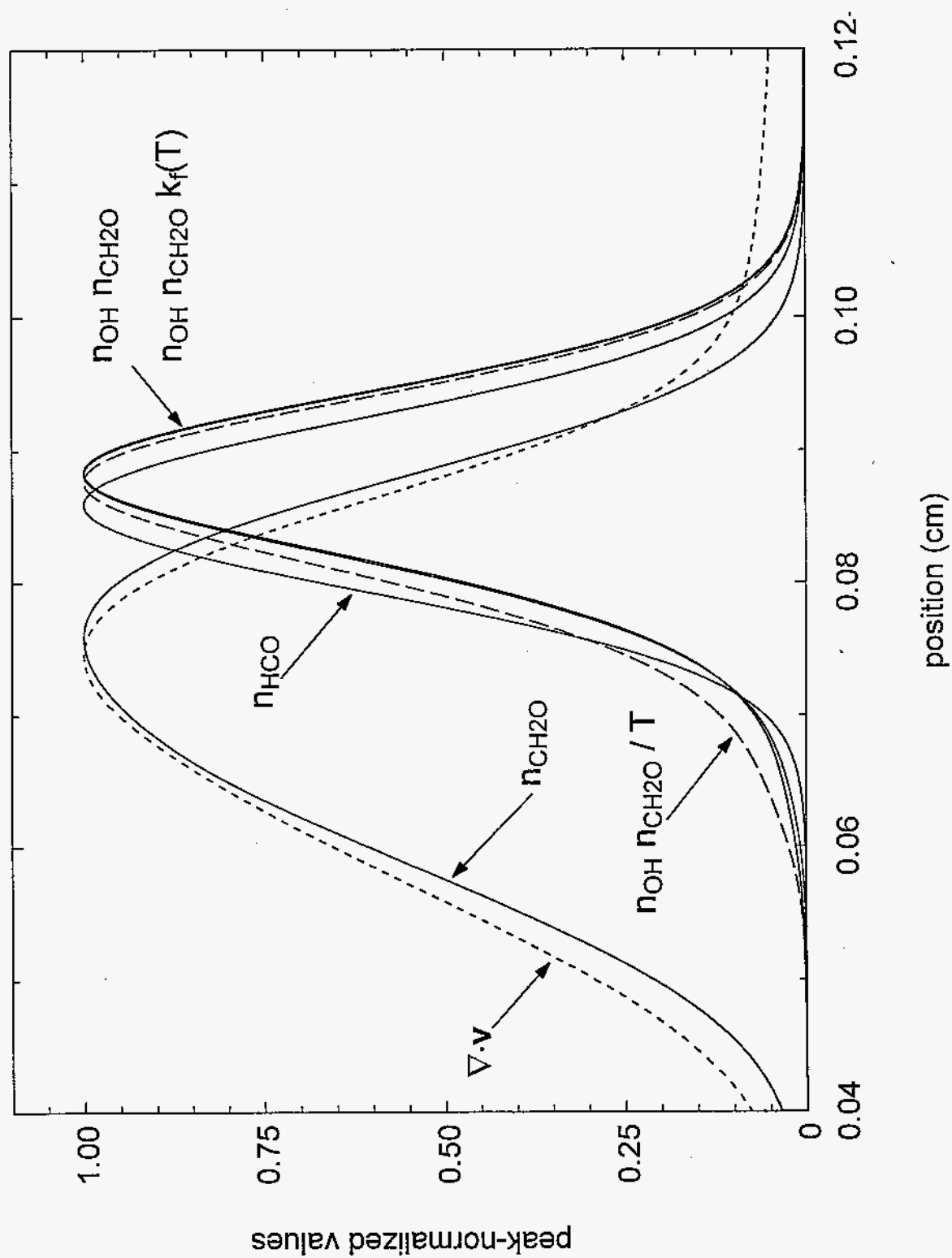
11

References

1. H. N. Najm, P. H. Paul, C. J. Mueller and P. S. Wyckoff, 'On the adequacy of certain experimental observables a measurements of heat release rate,' (to appear in Comb. and Flame, 1997).

2. N. T. Clemens and P. H. Paul, Comb. and Flame **102**, 271-284 (1995).

3. Q.-V. Nguyen and P. H. Paul, 26th Symposium (International) on Combustion (The Combustion Inst., Pitts. PA, 1996) pp. 357-364.

4. H. N. Najm, P. S. Wyckoff and O. M. Knio, 'Effect of equivalence ratio on premixed flame response to unsteady strain and curvature,' (submitted to 27th Symposium on Combustion, 1997).

5. M. Frenklach, H. Wang, M. Goldenberg, G. P. Smith, D. M. Golden, C. T. Bowman, R. K. Hanson, W. C. Gardiner and V. Lissianski (Gas Research Inst., 1995), topical report GRI-95/0058.

6. W. Tang and R. F. Hampson, J. Phys. Chem. Ref. Data **15**, 1087 (1986).

7. P. H. Paul, J. A. Gray, J. L. Durant and J. W. Thoman, AIAA J. **32**, 1670-1675 (1994).

8. J. E. Harrington and K. C. Smyth, Chem. Phys. Lett. **202**, 196-202 (1993).

9. B. Bauerle, J. Warnatz and F. Behrendt, 26th Symposium (International) on Combustion (The Combustion Inst., Pitts. PA, 1996) pp. 2619-2626.

10. R. G. Miller and E. K. C. Lee, J. Chem. Phys. **68**, 4448-4454 (1978).

11. C. M. L. Kerr, D. C. Moule and D. A. Ramsey, Can. J. Phys. **61**, 6-14 (1983).

12. K. Shibuya and E. K. C. Lee, J. Chem. Phys. **69**, 758-766 (1978).

13. P. H. Paul, J. Quant. Spectrosc. Radiat. Tranfer **51**, 511-524 (1994). P. H. Paul, J. Phys. Chem. **99**, 8472-8476 (1995).

14. P. H. Vaccaro, F. Temps, S. Halle, J. L. Kinsey and R. W. Field, J. Chem. Phys. **88**, 4819-4826 (1988).

15. D. V. Rogers and J. A. Roberts, J. Mol. Spec. **46**, 200-212 (1973).

16. J. M. F. van Dijk, M. J. H. Kemper, J. H. M Kerp and H. M. Buck, J. Chem. Phys. **69**, 2453-2461 (1978).

17. D. J. Clothier and D. A. Ramsey, Ann. Rev. Phys. Chem. **34**, 31-48 (1983).

18. G. K. Moortgart and P. Warneck, J. Phys. Chem. **70**, 3639-3651 (1979), and references therein.

19. H. J. Curran, W. J. Pitz, C. K. Westbrook, P. Dagaut, J-C Boettner and M. Cathonnect, 'A wide range modeling study of dimethyl ether oxidation,' (to appear in Int. J. of Chem. Kinetics 1998).
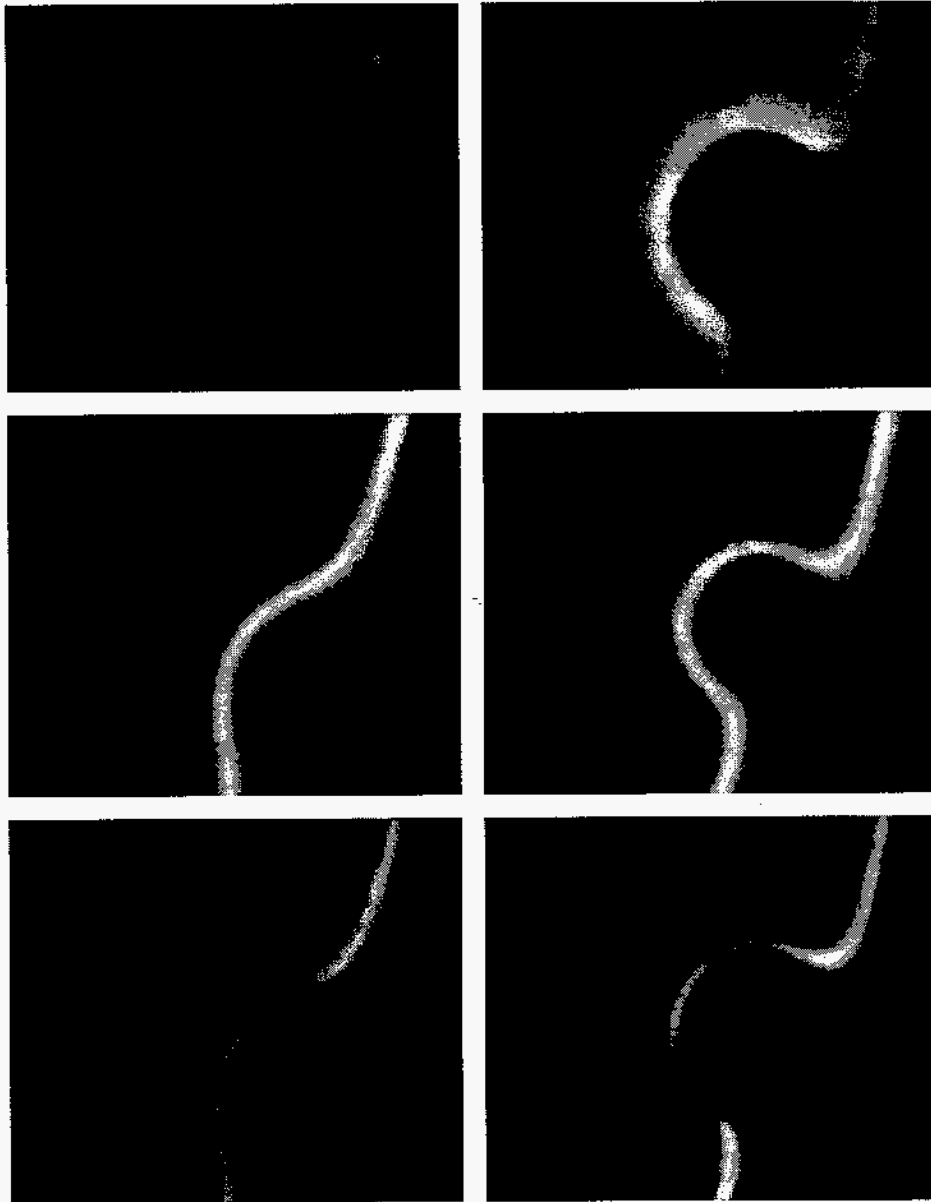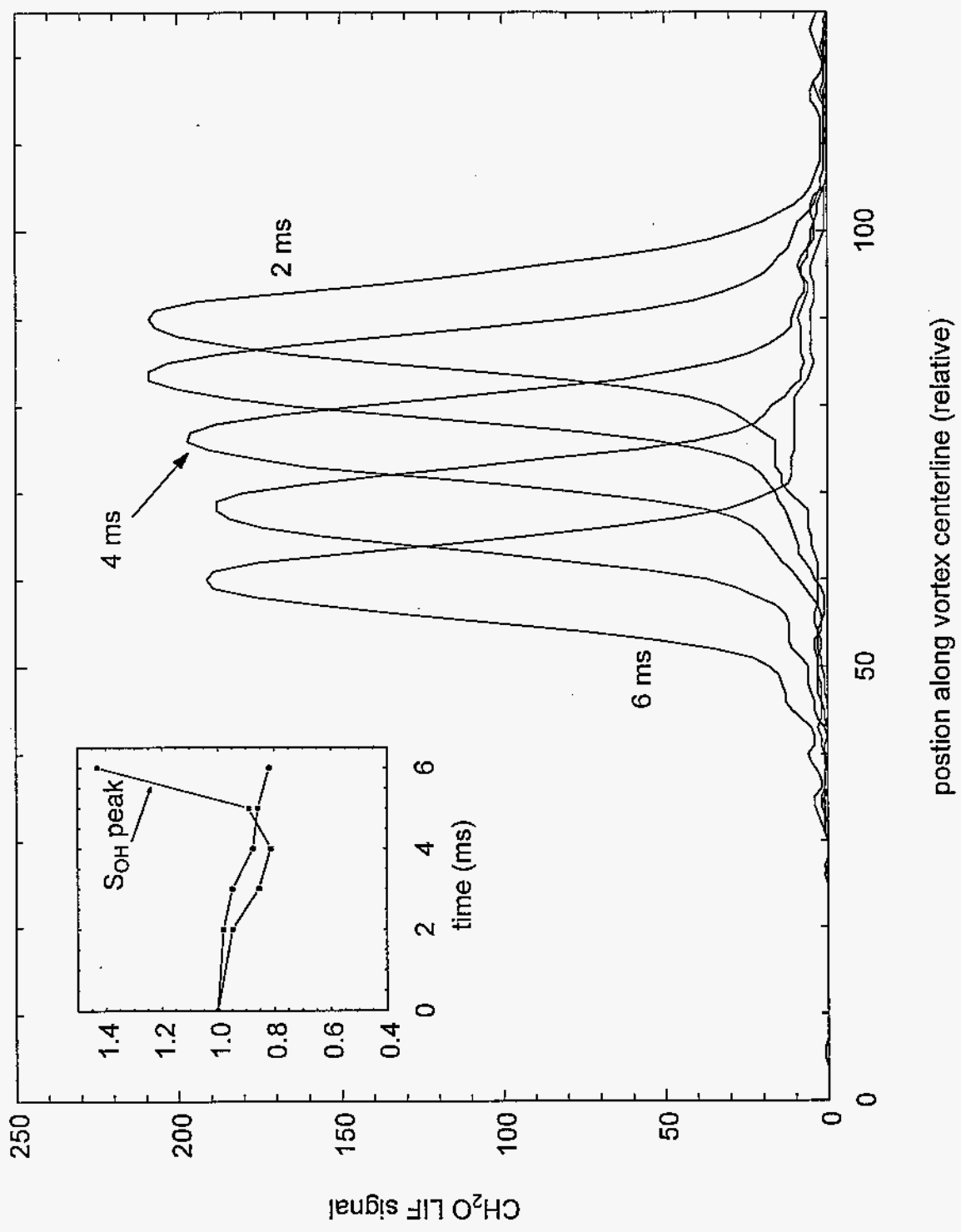
Figure Captions

Figure 1.   Time variation of peak heat release rate, HCO concentration and the product of OH and CH_2O concentrations. Taken on the centerline from a computed [4] 2D counter-rotating vortex-pair colliding with a laminar premixed flame (CH_4 - air, $\phi = 1$ and 1.2, 20% N_2 dilution). Values normalized to the values in the undisturbed flame.

Figure 2.   Spatial profiles of dilatation, CH_2O and HCO number densities and several possible representations for product of OH and CH_2O LIF signals for conditions of a laminar, freely propagating, premixed methane-air flame ($\phi = 1$).

Figure 3.   PLIF images of OH (top), CH_2O (middle) and the product (bottom row) taken at 2 (left) and 6 ms (right) into the interaction of a line vortex pair with a laminar V-flame. Field of view 20 by 17 mm. The color table is linear running from black (low) to white (high signal).

Figure 4.   Spatial profiles of S_{CH2O} taken along the vortex-pair centerline from the image data set (shown in part in figure 3). The inset shows the time evolution of the spatial integral of the CH_2O signal profiles and the peak OH signal on centerline as normalized to values in the undisturbed flame.

Figure 5.   Spatial profiles of product $S_{OH}S_{CH2O}$ taken along the vortex-pair centerline from the image data set (shown in part in figure 3). The inset shows the time evolution of the spatial integral of the profiles as normalized to the values in the undisturbed flame.

Figure Y.Γ.Ι

Fig. 7

peak-normalized values

position (cm)

n_{OH} n_{CH2O}

n_{OH} n_{CH2O} $k_f(T)$

n_{HCO}

n_{CH2O}

n_{OH} n_{CH2O} / T

$\nabla \cdot v$

paul & najm fig. 3

CH$_2$O LIF signal

position along vortex centerline (relative)

2 ms

4 ms

6 ms

S$_{OH}$ peak

time (ms)

Inset axes: product of OH and CH$_2$O LIF signals (vertical), distance along vortex centerline (relative) (horizontal). Curves labeled 2 ms, 4 ms, and 6 ms. Inset plot: vertical axis 0.4 to 1.0, horizontal axis time (ms) 0 to 6.
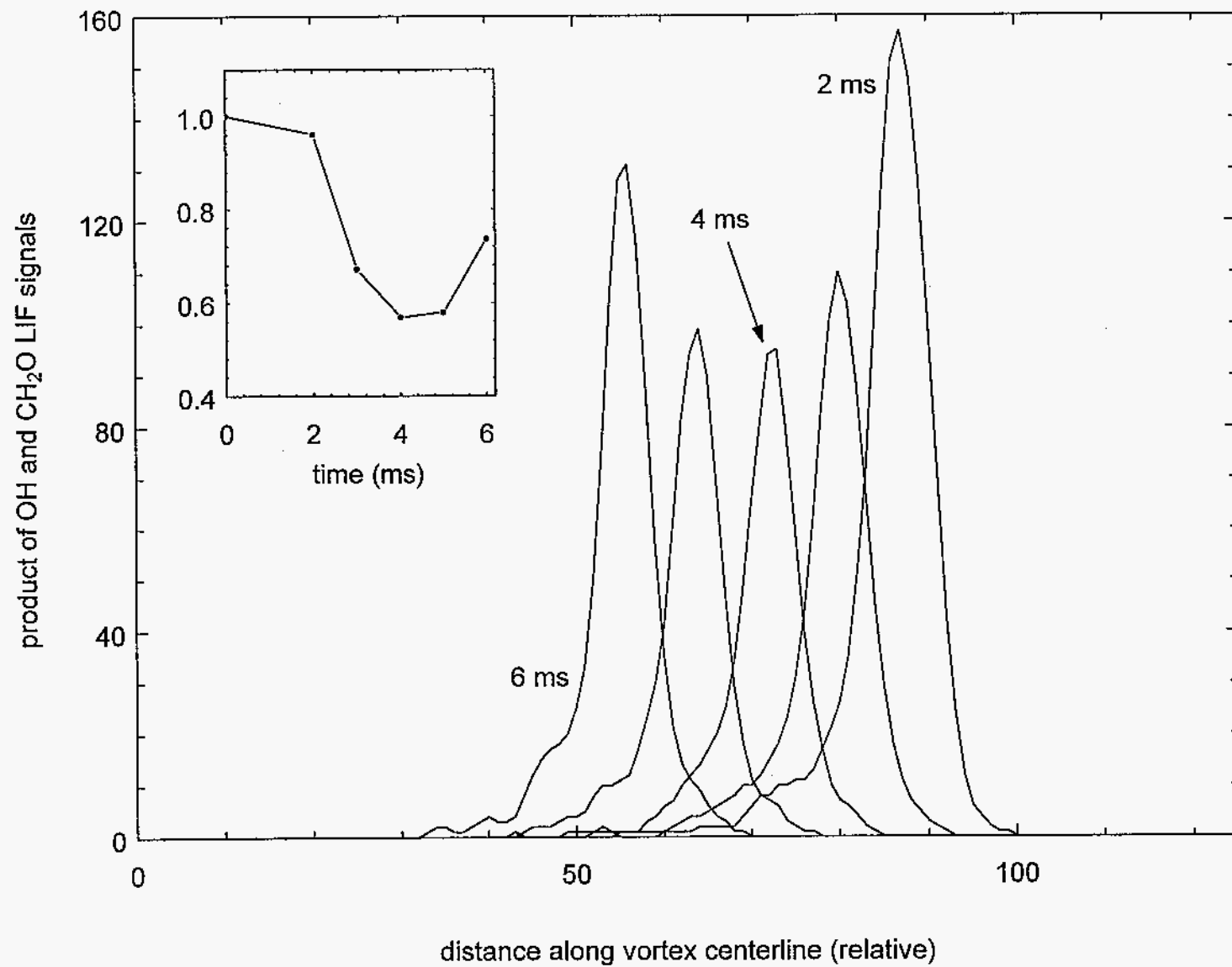
Report Number (14) $SAND--98-8474C$

$conf-980804---$

Publ. Date (11) $1997/12/12$
Sponsor Code (18) $DOE/EE, XF$
UC Category (19) $UC-1409, DOE/ER$

19980707 076

DOE